Available online at www.sciencedirect.com

ScienceDirect

www.elsevier.com/locate/jes

JES JOURNAL OF ENVIRONMENTAL SCIENCES www.jesc.ac.cn

Characterization of particulate products for aging of ethylbenzene secondary organic aerosol in the presence of ammonium sulfate seed aerosol

Mingqiang Huang[1,2,3], *Jiahui Zhang*[1], *Shunyou Cai*[1,2], *Yingmin Liao*[3], *Weixiong Zhao*[4], *Changjin Hu*[4], *Xuejun Gu*[4], *Li Fang*[4], *Weijun Zhang*[4,*]

1. *College of Chemistry & Environment, Minnan Normal University, Zhangzhou 363000, China. E–mail: huangmingqiang@gmail.com*
2. *Fujian Province Key Laboratory of Modern Analytical Science and Separation Technology, Zhangzhou 363000, China*
3. *Department of Environmental Science and Engineering, Xiamen University, Tan Kah Kee College, Zhangzhou 363105, China*
4. *Laboratory of Atmospheric Physico-Chemistry, Anhui Institute of Optics and Fine Mechanics, Chinese Academy of Sciences, Hefei 230031, China*

ARTICLE INFO

Article history:
Received 8 August 2015
Revised 15 November 2015
Accepted 27 November 2015
Available online 25 March 2016

Keywords:
Ethylbenzene
Secondary organic aerosol
$(NH_4)_2SO_4$ seed aerosol
Laser desorption/ionization
Fuzzy clustering (FCM) algorithm
Aging mechanism

ABSTRACT

Aging of secondary organic aerosol (SOA) particles formed from OH– initiated oxidation of ethylbenzene in the presence of high mass (100–300 μg/m^3) concentrations of $(NH_4)_2SO_4$ seed aerosol was investigated in a home-made smog chamber in this study. The chemical composition of aged ethylbenzene SOA particles was measured using an aerosol laser time-of-flight mass spectrometer (ALTOFMS) coupled with a Fuzzy C-Means (FCM) clustering algorithm. Experimental results showed that nitrophenol, ethyl-nitrophenol, 2,4-dinitrophenol, methyl glyoxylic acid, 5-ethyl-6-oxo-2,4-hexadienoic acid, 2-ethyl-2,4-hexadiendioic acid, 2,3-dihydroxy-5-ethyl-6-oxo-4-hexenoic acid, 1H-imidazole, hydrated N-glyoxal substituted 1H-imidazole, hydrated glyoxal dimer substituted imidazole, 1H-imidazole-2-carbaldehyde, N-glyoxal substituted hydrated 1H-imidazole-2-carbaldehyde and high-molecular-weight (HMW) components were the predominant products in the aged particles. Compared to the previous aromatic SOA aging studies, imidazole compounds, which can absorb solar radiation effectively, were newly detected in aged ethylbenzene SOA in the presence of high concentrations of $(NH_4)_2SO_4$ seed aerosol. These findings provide new information for discussing aromatic SOA aging mechanisms.

Introduction

Ethylbenzene and other aromatic hydrocarbons that are released into the atmosphere by human activities, such as motor vehicle exhaust and evaporation of solvents, are important volatile organic compounds in urban air (Correa et al., 2012; Lan and Minh, 2013; Bolden et al., 2015). Besides its toxicity to humans, conversion of ethylbenzene in the atmosphere can play a significant role in the formation of secondary organic aerosol (SOA) (Sato et al., 2010; Ziemann and Atkinson, 2012; Schnitzler et al., 2014). Aromatic SOA particles have lifetimes of about 1 week (Balkanski et al., 1993; Rudich et al., 2007), during which they can undergo continuous reaction with reactive species, nitrogen oxides and other

* *Corresponding author*. E-mail: wjzhang@aiofm.ac.cn (Weijun Zhang).

http://dx.doi.org/10.1016/j.jes.2015.11.033
1001-0742/

chemical substances, commonly called aging (Robinson et al., 2007; Rudich et al., 2007; Andreae, 2009). The chemical composition, volatility, hygroscopicity, toxicity, and optical properties change with SOA aging (Ng et al., 2011; Tritscher et al., 2011; Sareen et al., 2013). Aromatic SOA aging has attracted great attention because of the impacts of aged SOA on air visibility (Baltensperger, 2010; Singh and Dey, 2012), formation of clouds, climate change (Lee et al., 2014), and human health (Topinka et al., 2011; Sorooshian et al., 2012).

Over the past few years, studies on the effects of environmental factors on the optical properties of aged SOA and the identification of the aged products have been of particular interest (Updyke et al., 2012; Loza et al., 2012; Nakayama et al., 2013; Huang et al., 2014). The effects of ammonia and nitrogen oxides on the optical properties of aromatic aged SOA were investigated by Updyke et al. (2012) and Nakayama et al. (2013) using UV–Vis absorption spectra and cavity ring-down spectroscopy (CRDS), respectively, and the light-absorbing ability of the aged SOA was found to be enhanced with increasing initial NH_3 and NO_x concentrations. Recently, Loza et al. (2012) conducted a 36 hr *m*-xylene SOA aging chamber experiment, and observed that the O/C ratio of aged products gradually increased with the extension of time. Subsequently, Sato et al. (2012) and Huang et al. (2014) identified the nitrophenol, oxocarboxylic acid and epoxide products of aged benzene SOA with liquid chromatography/time-of-flight mass spectrometry (LC/MS) and aerosol laser time-of-flight mass spectrometer (ALTOFMS), respectively.

It is well-known that aromatic SOA formation and aging are related to preexisting particles, and inorganic seed aerosol having relatively large surface area is one type of preexisting particle (Wang et al., 2011). However, the aromatic SOA aging experiments described above were carried out in the absence of inorganic seed aerosol. Ammonium sulfate ($(NH_4)_2SO_4$), which is formed by the reaction of ammonia with sulfuric acid, is one of the most common inorganic seed aerosols in the atmosphere (Robinson et al., 2013). With the rapid development of China's economy, the extensive use of the fossil fuel coal results in urban atmospheres containing a high concentration of SO_2 (Schreier et al., 2015). Meanwhile, China is a large agricultural country, and agricultural production and the livestock breeding industry emit large amounts of ammonia per year, resulting in high concentrations of ammonium sulfate in the urban atmosphere (Tong and Xu, 2012). For example, the annual average concentration of aerosol particles in Beijing is about 100 $\mu g/m^3$, and during haze days it may exceed 300 $\mu g/m^3$, one-third of which are inorganic ionic species (mainly SO_4^{2-}, NO_3^- and NH_4^+) (He et al., 2001; Wang et al., 2006). To the best of our knowledge, no investigations on the effects on the chemical composition of the aged aromatic SOA in the presence of high mass concentrations of $(NH_4)_2SO_4$ seed aerosol have been performed up to now.

Our group has used a vacuum ultraviolet photoionization mass spectrometer and aerosol time-of-flight mass spectrometer to measure the gas and particle phase products formed from photooxidation of ethylbenzene in real-time, and ethylphenol, methylglyoxal, phenol, benzaldehyde, and 2-ethylfurane were detected in both the gas and particle phases (Huang et al., 2010). Recently, the Fuzzy C-Means (FCM) algorithm has been developed by our group to classify the mass spectra of large numbers of particles obtained by ALTOFMS (Huang et al., 2013). The latest study demonstrated that FCM allowed a clear identification of twelve distinct chemical particle classes in aged 1,3,5-trimethylbenzene SOA, showing that the real-time ALTOFMS detection approach coupled with the FCM data processing algorithm can successfully carry out the cluster analysis of SOA (Huang et al., 2015). Based on this, we focus on the chemical characterization of particulate products that are formed upon formation of ethylbenzene SOA and subsequent aging through OH-initiated reactions in the presence of high mass (100–300 $\mu g/m^3$) concentrations of $(NH_4)_2SO_4$ seed aerosol using ALTOFMS coupled with the FCM algorithm in this study. The particulate products of the aged ethylbenzene SOA were obtained, and the possible reaction mechanisms leading to these aged products were also discussed.

1. Experimental method

1.1. Material

Ethylbenzene (>99%) was bought from Sigma-Aldrich Chemistry Corporation, Germany. Sodium nitrite (>99%), methanol (>99%) and ammonium sulfate (>99%) were obtained from The Third Reagent Factory of Tianjin. Nitric oxide (99.9%) was provided by Nanjing Special Gas Factory. Methyl nitrite was prepared and purified by the method provided in our previous studies (Huang et al., 2013, 2014, 2015), and preserved in liquid nitrogen until use.

1.2. Generation of $(NH_4)_2SO_4$ seed aerosols

$(NH_4)_2SO_4$ seed aerosol was generated by aspirating 0.001 mol/L salt solution (0.066 g $(NH_4)_2SO_4$ dissolved in 500 mL deionized water) through a constant output atomizer (TSI Inc. Model 3076), and subsequently passed through a diffusion dryer (TSI Inc. Model 3062) (with exiting RH lower than 20%) and ^{85}Kr charge neutralizer (TSI Inc., Model 3077) (removing charges to give neutral aerosol) before entering the smog chamber. The generated $(NH_4)_2SO_4$ seed aerosol was 10,000–50,000 particles/cm^3 with mean diameter of about 100 nm, and the concentration of the $(NH_4)_2SO_4$ seed aerosol in the smog chamber was established at about 100, 200, and 300 $\mu g/m^3$, respectively, by controlling the flow rate of zero air (Huang et al., 2013).

1.3. Smog chamber experiment on ethylbenzene SOA aging

Aging of ethylbenzene SOA was performed using UV-irradiation of ethylbenzene/CH_3ONO/NO/air mixtures in the absence and presence of 100, 200 and 300 $\mu g/m^3$ of dry $(NH_4)_2SO_4$ seed aerosol in an 850 L sealed collapsible polyethylene smog chamber (Huang et al., 2012, 2013, 2014). In all experiments, the temperature and relative humidity in the smog chamber were measured continuously by a temperature and humidity sensor (Vaisala HMT333, Finland). The temperature and relative humidity in the chamber was maintained at about 25 ± 4°C and 15 ± 2%, respectively. After flushing the smog chamber and obtaining the desired $(NH_4)_2SO_4$ seed aerosol concentration, ethylbenzene, NO and CH_3ONO were introduced into the smog

chamber, then the chamber was filled with the purified air to full volume. The concentration of ethylbenzene, CH_3ONO, and NO was 2.0, 20.0, and 2.0 ppm, respectively. Then, 4 UV lamps were turned on and the photooxidation reaction was initiated. OH radicals were generated by the irradiation of CH_3ONO with UV lamps with wavelength in range of 300–400 nm (Atkinson et al., 1981). In each experiment, the OH concentration reached a maximum immediately after turning on the UV lamps and then decreased with time, but the OH concentration maintained a level > 5×10^5 molecules/cm^3 after 24 hr photooxidation, indicating that the particles and vapors in the reaction chamber were continuously oxidized during irradiation (Huang et al., 2014, 2015). To achieve longer OH exposure times with all instrument sampling, the concentrations of ethylbenzene, NO_x, O_3 and the volume concentration and mobility size distributions of SOA particles were measured by a GC–FID (Agilent 7820A, USA), NO–NO_2–NO_x analyzer (TEI model 42i), O_3 analyzer (TEI model 49i) and scanning mobility particle sizer (SMPS; TSI 3080L DMA, TSI 3775 CPC) every 30 min, respectively. After a period of photooxidation, the aged ethylbenzene SOA particles were analyzed continuously using the ALTOFMS connected directly to the chamber using a Teflon line. Then, the obtained aged particles were Fuzzy C-Means algorithm (FCM) (Bezdek, 1981) clustered based on their individual mass spectra as described in detail in our previous studies (Huang et al., 2013, 2014, 2015).

2. Results and discussion

2.1. Formation and aging of ethylbenzene SOA particles

The time series of the ethylbenzene, NO_x, O_3 and SOA mass concentrations (corrected for wall-loss correction) measured are shown in Fig. 1. A density of 1.23 g/cm^3, calculated by comparing the electronic mobility diameter from the SMPS and vacuum aerodynamic diameter from ALTOFMS, was employed to estimate SOA mass concentrations (Huang et al., 2015). For the seeded experiments, SOA mass concentrations were obtained by subtracting the initial seed aerosol mass concentrations. SOA mass was corrected for wall loss assuming a first-order loss rate calculated by fitting the particle number concentration decay at the end of each experiment (Huang et al., 2015). As shown in Fig. 1, less than 30 min after turning on the UV lamps, monomodal SOA formation could be detected using a SMPS measurement. This aerosol grew in number of particles and mass for the first 30 min and then reached a maximum at 6 hr, when no ethylbenzene was left in the chamber according to GC data. Before 6 hr in these experiments, when there were sufficient ethylbenzene and OH radicals to generate many more SOA particles than were lost, we observed the mass increase. Afterwards, however, there was no ethylbenzene available in

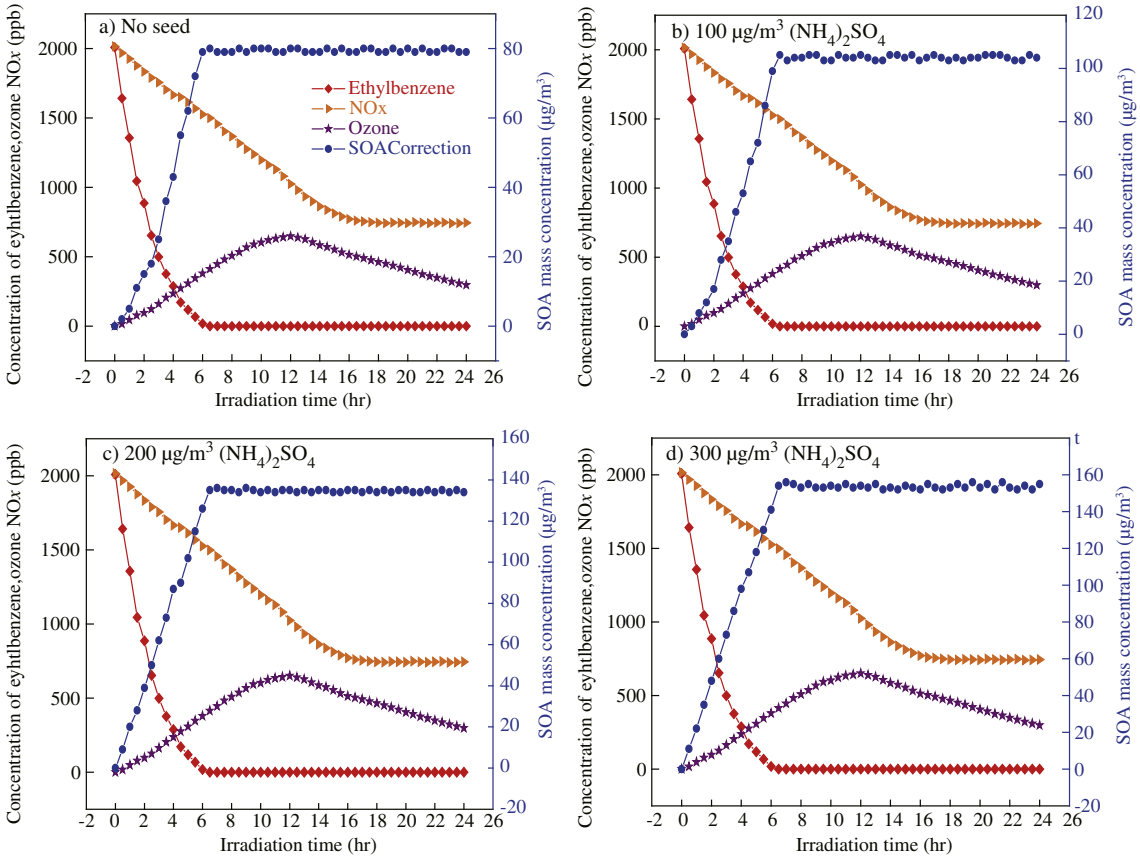

Fig. 1 – Ethylbenzene, NO_x, O_3 and SOA mass concentrations (corrected for wall-loss) measured as a function of irradiation time in the presence of (a) no seed, (b) 100 μg/m^3$(NH_4)_2SO_4$, (c) 200 μg/m^3 $(NH_4)_2SO_4$ and (d) 300 μg/m^3 $(NH_4)_2SO_4$. SOA: secondary organic aerosol.

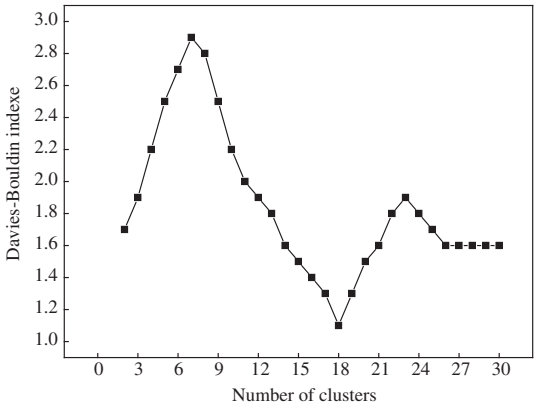

Fig. 2 – Clustering number evaluated using the Davies–Bouldin index for the aged ethylbenzene SOA particles in the presence of 100 μg/m^3 $(NH_4)_2SO_4$ seed aerosol after 24 hr photooxidation. SOA: secondary organic aerosol.

the smog chamber, SOA aging processes occurred, and the aged ethylbenzene SOA particles deposited onto the chamber wall due to turbulence, Brownian diffusion and gravitational sedimentation of particles (Bowman et al., 1997), causing aerosol losses.

According to Fig. 1, the change of NO_x and O_3 concentration with time, as well as ethylbenzene consumption, was nearly the same throughout these four experiments. However, the corrected maximum mass concentration of SOA in the presence of 100, 200 and 300 μg/m^3 of $(NH_4)_2SO_4$ seed aerosol was 105, 136 and 154 μg/m^3, respectively, higher than that observed for the unseeded experiment of 80 μg/m^3, indicating that the presence of high concentrations of $(NH_4)_2SO_4$ seed aerosol has no obvious effect on O_3 formation, but it does enhance ethylbenzene SOA generation. These results are consistent with the findings reported by Lu et al. (2009), that *m*-xylene SOA yield was enhanced in the presence of high concentrations of $(NH_4)_2SO_4$ seed aerosol. The effects on the chemical composition of the aged ethylbenzene SOA in the presence of $(NH_4)_2SO_4$ seed aerosol are discussed in the following sections.

2.2. Classification of the spectra of aged ethylbenzene SOA particles

As shown in our previous studies (Huang et al., 2012, 2013, 2014), a mass spectrum is only acquired for particles whose diameter has been measured by ALTOFMS. The obtained mass spectra of single particles are described as 300-dimensional data vectors, using the ion masses as dimensions and the ion signal peak areas as values. The data vectors of all particles measured are written into a classification matrix. The data for each spectrum is stored as one row in this matrix. Basically, the FCM algorithm calculates a fuzzy partition matrix to group some of the data points into *k* clusters, and the membership coefficients u_{ik} of each particle *i* to each class center *k* are determined. The class centers and membership coefficients provide for a detailed characterization of all the measured particles. Each class center can be represented as a "mean" mass spectra pattern. This provides for the characterization of the mean chemical composition of the particle class. FCM computes the Davies–Bouldin index to evaluate the optimum cluster number among different partitions. Small values of Davies–Bouldin correspond to clusters that are compact, and whose centers are far away from each other. Consequently, the number of clusters that minimizes Davies–Bouldin is taken as the optimal number of clusters (Huang et al., 2013, 2014).

About 6500 pieces of single particle mass spectra of the aged ethylbenzene SOA particles in the presence of 100 μg/m^3 $(NH_4)_2SO_4$ seed aerosol at different photooxidation times were obtained. After setting the FCM initial clustering number (*n*) from 2 to 30, the fuzzy degree parameter (*m*) to 2, the maximum number of cycles to 500, and the precision of the clustering to 0.1, the obtained mass spectra were processed with the FCM algorithm to extract out potential aerosol. Figs. 2 and S1 in Appendix A. Supplementary data show the Davies–Bouldin index for the ethylbenzene SOA particles in the presence of 100 μg/m^3 $(NH_4)_2SO_4$ seed aerosol at different photooxidation times. For 24 hr photooxidation, 6518 pieces of single particle mass spectra of the aged ethylbenzene SOA particles were obtained, and the Davies–Bouldin index displayed in Fig. 2 has the minimum value at $n = 18$, suggesting that these aged SOA particles can be clustered into 18 classes. Figs. 3 and S2–S6 in Appendix A. Supplementary data exhibit the spectra patterns determined for the cluster centers at different photooxidation times. The spectral patterns are displayed in analogy to real time-of-flight mass spectra of aromatic SOA particles obtained in our previous studies (Huang et al., 2007, 2012, 2013) as positive ion "signals", with the signal intensities representing the vector components of the cluster center.

2.3. Chemical composition and mechanism of aged ethylbenzene SOA particles

The mass spectrum of class 1 at different photooxidation times contains only the peak of *m*/z 18, which is usually representative of ammonium (NH_4^+) (Kane and Johnston, 2001; Garland et al., 2005) or water ion (Alfarra et al., 2006). In order to verify whether the *m*/z 18 is derived from the gas phase water molecules of the purified air, the chamber was filled with purified air to full volume, and the relative humidity in the smog chamber was 16%. Then, the purified air in the smog chamber was analyzed continuously using the ALTOFMS connected directly to the chamber using a Teflon line. However, no mass spectrum was obtained by ALTOFMS, indicating that *m*/z 18 may be derived from ammonium ion. To further confirm this inference, $(NH_4)_2SO_4$ particles were generated as described in the experimental methods, and measured by ALTOFMS. The laser desorption/ionization (LDI) mass spectrum of the average of 100 single $(NH_4)_2SO_4$ particles is shown in Fig. 4, which is different from those obtained by Garland et al. (2005) and Kane and Johnston (2001). The mass spectrum of $(NH_4)_2SO_4$ particles measured by Garland et al. (2005) is dominated by fragments at *m*/z 17 and 16 under ionization, and the ratio of mass 17 to 16 is close to 1.1. However, the LDI mass spectrum of $(NH_4)_2SO_4$ particles measured by Kane and Johnston (2001) was quite complicated. Besides the peaks of *m*/z 18, 17, and 16, *m*/z 12, 24, 30, 32, and 48 were observed. Also, the intensity of *m*/z 18 was larger than *m*/z 17 and *m*/z 16, respectively.

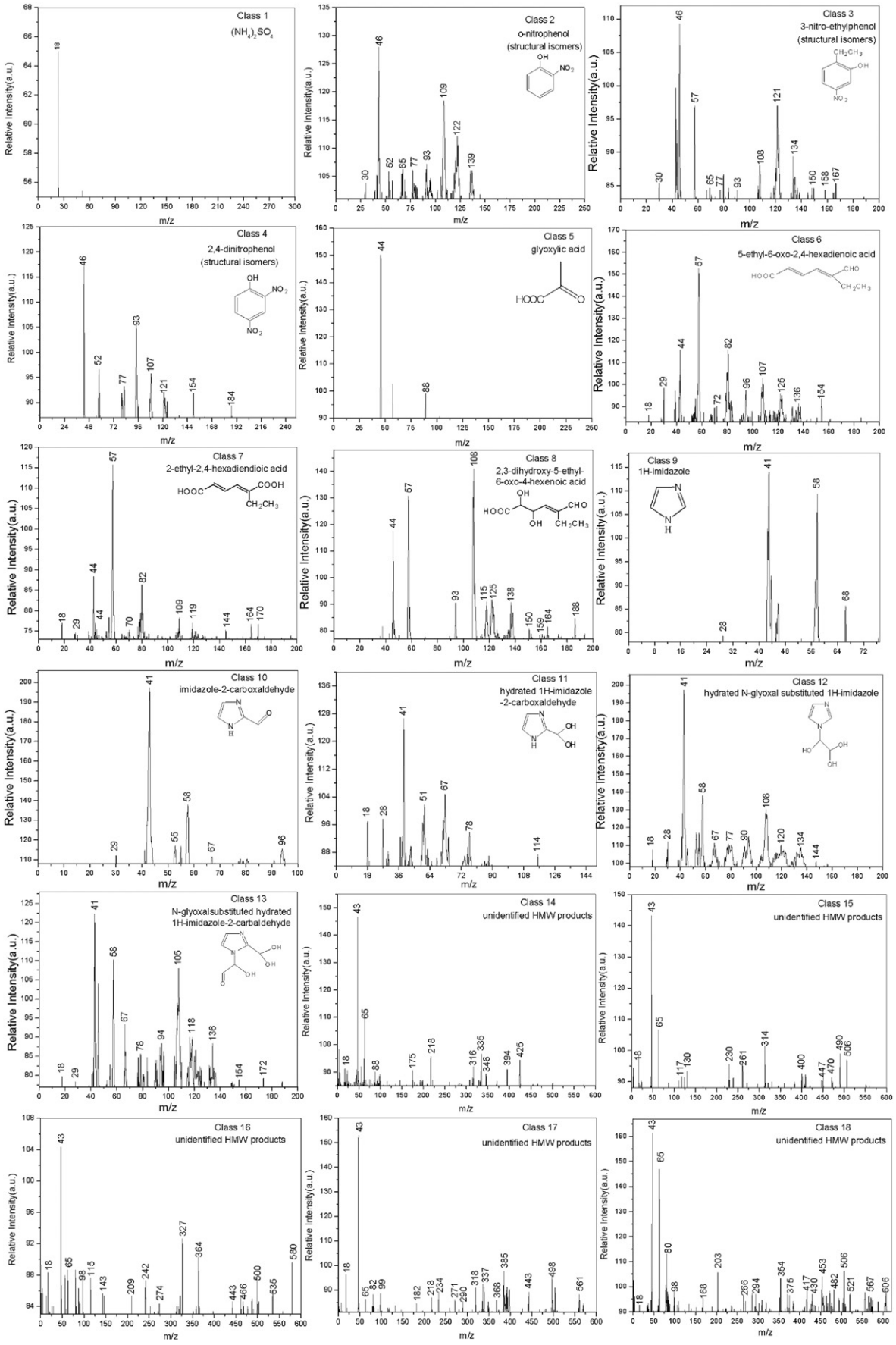

Fig. 3 – Representative spectral patterns of the aged ethylbenzene SOA particles in the presence of $(NH_4)_2SO_4$ seed aerosol after 24 hr photooxidation determined by FCM. SOA: secondary organic aerosol; FCM: Fuzzy C-Means.

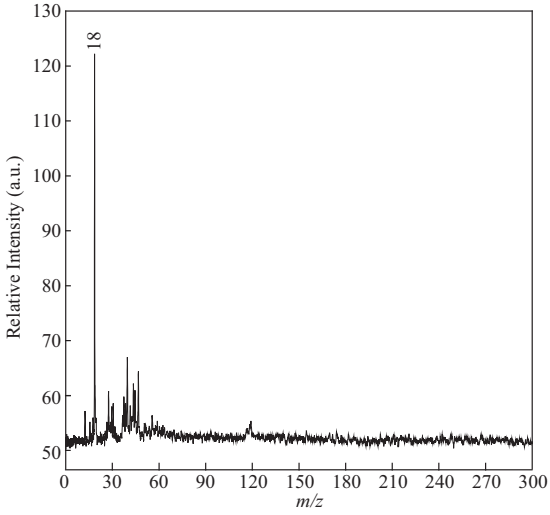

Fig. 4 – Laser desorption/ionization mass spectra of the average of 100 single $(NH_4)_2SO_4$ particles.

It is worth noting that the mass spectra of $(NH_4)_2SO_4$ particles mentioned above were obtained with different ionization sources. The mass spectrum of $(NH_4)_2SO_4$ particles was detected by Garland et al. (2005) with aerosol mass spectrometry, and the $(NH_4)_2SO_4$ vapor plume was ionized using a 70 eV electron impact (EI) ionization source. Kane and Johnston (2001) used laser ablation aerosol mass spectrometry to measure the mass spectrum of $(NH_4)_2SO_4$ particles, and an ArF excimer laser at 193 nm with a 8 nsec, 2.5 mJ pulse was utilized for ablation and ionization of the particles. The laser was focused with a 20 cm lens to give a fluence of 2.0×10^4 J/m^2 in the mass spectrometer source region. ALTOFMS is similar to laser ablation aerosol mass spectrometry, but the ionization source is the pulsed excimer KrF laser at 248 nm having a pulse length 2.5 nsec and an average power density of 10^3 J/m^2 (Huang et al., 2007), whose energy is much less than that of the ArF excimer laser. The KrF excimer laser may not be able to cause the cleavage of ammonium or sulfate ion, thus, only *m*/z 18 was found in the LDI mass spectrum of $(NH_4)_2SO_4$ particles in this study. Hence, the intense signal at *m*/z 18 is representative of ammonium ion, and the mass spectrum of class 1 contains only the peak of *m*/z 18, corresponding to the $(NH_4)_2SO_4$ particles.

According to the main fragments of each class and possible reaction pathways of ethylbenzene with OH radicals, the speculated molecular structures of the oxidation products are shown in Figs. 3 and S2–S6 in Appendix A. Supplementary data. It can be seen that the spectral patterns for the cluster centers at 2, 6, 12, 18, 22 and 24 hr photooxidation are different from each other, indicating that the chemical compositions of ethylbenzene SOA were modified continually upon aging. For the 2 hr photooxidation, phenol, benzaldehyde, ethylphenol, and benzoic acid are the major components in the ethylbenzene SOA. As mentioned above, the mass concentration of SOA reached a maximum at 6 hr, and the first-generation products of glyoxal, glyoxylic acid, phenol, ethylglyoxylic acid, benzaldehyde, benzoic acid, ethylphenol, 5-ethyl-6-oxo-2,4-hexadienal, and ethyl-nitrophenol, which were previously observed by Forstner et al. (1997) and our previous ethylbenzene photooxidation experiment (Huang et al., 2010); while afterwards, SOA aging processes occur, and new aged products are formed at 12, 18, 22 and 24 hr photooxidation. However, after 22 hr photooxidation, in addition to high-molecular-weight (HMW) products, the other aged components remain unchanged. The chemical composition and formation mechanism of the aged products after 24 hr photooxidation are discussed as follows.

The characteristic cleavage fragment peak *m*/z 46 (NO_2^+), benzene ion peak *m*/z 77 ($C_6H_5^+$), and benzene fragment ion peaks at *m*/z 65 ($C_5H_5^+$), 52 ($C_4H_4^+$) and 39 ($C_3H_3^+$) were found in the mass spectrum of the second to fourth class as displayed in Fig. 3, so were tentatively identified as aromatic nitrogen-containing organic compounds (Silva and Prather, 2002; Alfarra et al., 2006; Huang et al., 2014, 2015). In addition to our previously detected ethyl-nitrophenol, *o*-nitrophenol (or *p*-nitrophenol) and 2,4-dinitro phenol were newly found in the presence of 100 μg/m^3 $(NH_4)_2SO_4$ seed aerosol. The formation of the photooxidation products of phenolic compounds, such as 2-ethyl phenol and phenol, have been previously reported in a number of ethylbenzene chamber studies (Yu et al., 1997; Forstner et al., 1997; Huang et al., 2010). According to the theory of Henry and Donahue (2012), SOA aging includes OH-radical oxidation of the photooxidation products. As shown in Fig. 5, OH can react with 2-ethylphenol and phenol to abstract an H-atom from the hydroxyl group to form 2-ethyl-phenoxy radical and phenoxy radical, respectively. As proposed by Forstner et al. (1997), these two phenoxy radicals can then react with NO_2 to form a variety of nitro phenolic compounds. The positions of the alkoxy radical determine where NO_2 adds to the ring. OR groups on an aromatic ring are ortho- and para- directing, with OR more strongly activating. Hence, NO_2 adds ortho and para to the oxygen in the phenoxy radical. This step leads to the formation of *o*-nitro-phenol, *p*-nitro-phenol, 2-ethyl-4-nitro-phenol and 2-ethyl-6-nitro-phenol, respectively. Also shown in Fig. 5 are further reactions of *o*-nitro-phenol (or *p*-nitro-phenol) with OH and NO_2 to yield 2,4-dinitrophenol, another species detected in the aged ethylbenzene SOA.

The fifth to eighth classes contain the characteristic cleavage fragment peak of *m*/z 44 (CO_2^+), demonstrating that these clusters contain carboxylic acids (Alfarra et al., 2006; Huang et al., 2014, 2015). Carbonyl compounds such as methylglyoxal and 2-ethyl-6-oxo-2,4-hexadienal, which are produced as ring-opened products from the reaction of ethylbenzene with OH radicals, have been measured in the gas and particle phase products of previous ethylbenzene chamber experiments (Yu et al., 1997; Forstner et al., 1997; Huang et al., 2010). The experimental results of Sato et al. (2012) indicate that SOA aging proceeds through the oxidation of the internal double bond of ring-opened products and carboxylic acid formation resulting from the oxidation of the carbonyl group. As shown in Fig. 6, OH abstracts a hydrogen atom from the carbonyl group, and oxygen adds to the radical. This peroxy radical can react with HO_2 (or RO_2) to form methyl glyoxylic acid and 5-ethyl-6-oxo-2,4-hexadienoic acid, respectively. The latter may further react with OH radical, O_2 and HO_2 (or RO_2) to generate 2-ethyl-2,4-hexadiendioic acid, or may undergo the OH radical oxidation shown in Fig. 6 to

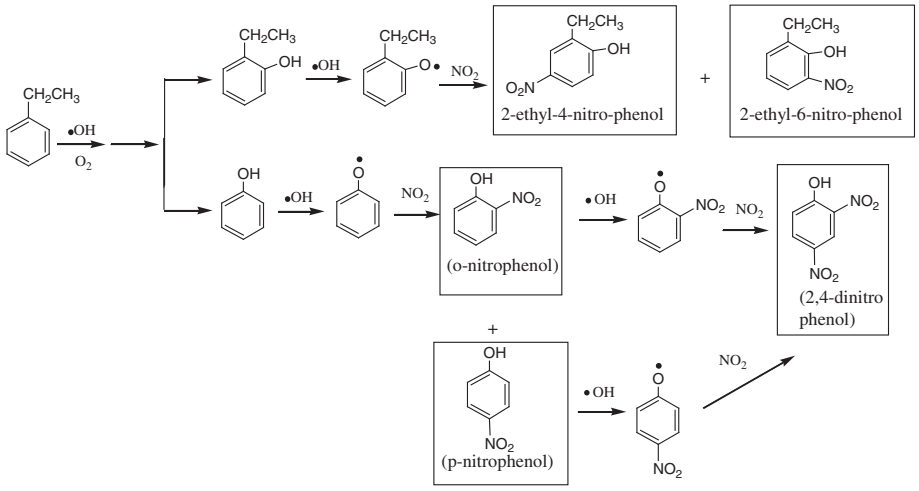

Fig. 5 – Proposed aging mechanism leading to the formation of aromatic nitrogen-containing organic compounds.

produce 2,3-dihydroxy-5-ethyl-6-oxo-4-hexenoic acid and to propagate the aging reaction (Forstner et al., 1997; Sato et al., 2012).

The mass spectra of the 9th to 13th classes have the characteristic cleavage fragment peaks *m*/*z* 41 ($C_2H_3N^+$) and *m*/*z* 67 ($C_3H_3N_2^+$), indicating that these clusters belong to the imidazole compounds (Yu et al., 2011; Kampf et al., 2012). The clustering results show that high mass concentrations of $(NH_4)_2SO_4$ seed aerosol can promote the formation of imidazole compounds in aged ethylbenzene SOA. According to the experimental results of Meyer et al. (2009), $(NH_4)_2SO_4$ seed aerosol can form ammonium ion (NH_4^+) by absorbing water from its outer organic layer coating. Ammonium is a weak acid with dissociation constant K_a of 5.6×10^{-10} ($pK_a = 9.25$), it is very difficult to hydrolyze to generate hydronium ($NH_4^+ + H_2O \rightarrow NH_3 + H_3O^+$) (Rincón et al., 2009). However, ammonium ion was found to react with α-dicarbonyl compounds, such as glyoxal and methyl glyoxal to form imidazole products in previous experiments (Nozière et al., 2009; Yu et al., 2011; Kampf et al., 2012). Previous studies have indicated that glyoxal is the major aldehyde product formed from OH-initiated oxidation of ethylbenzene (Yu et al., 1997; Forstner et al., 1997; Huang et al., 2010), and the generated glyoxal could condense on existing $(NH_4)_2SO_4$ seed aerosols. As shown in Fig. 7, ammonium ion acts as in two ways *i.e.*, by acting as a Bronsted acid (*i.e.*, releasing protons) or forming covalent nitrogen species such as imminium intermediates (Nozière et al., 2009; Yu et al., 2011; Kampf et al., 2012). Accordingly, in the latter pathway of this mechanism, glyoxal is protonated by the ammonium ion, and the protonated glyoxal can undergo nucleophilic attack by ammonia followed by loss of water and H^+ ion, giving the diimine (1). In the other pathway, glyoxal is protonated by the ammonium ion and subsequently hydrolyzed by diol product (2) and tetrol product (3) formation, respectively (Nozière et al., 2009; Yu et al., 2011; Kampf et al., 2012).

Diimine (1) reacts with tetrol product (3) to produce (4) via the dehydration reaction of the hydrogen atom of the amido of (1) and the OH of (3). Product (4) is unstable, so that the lone pair

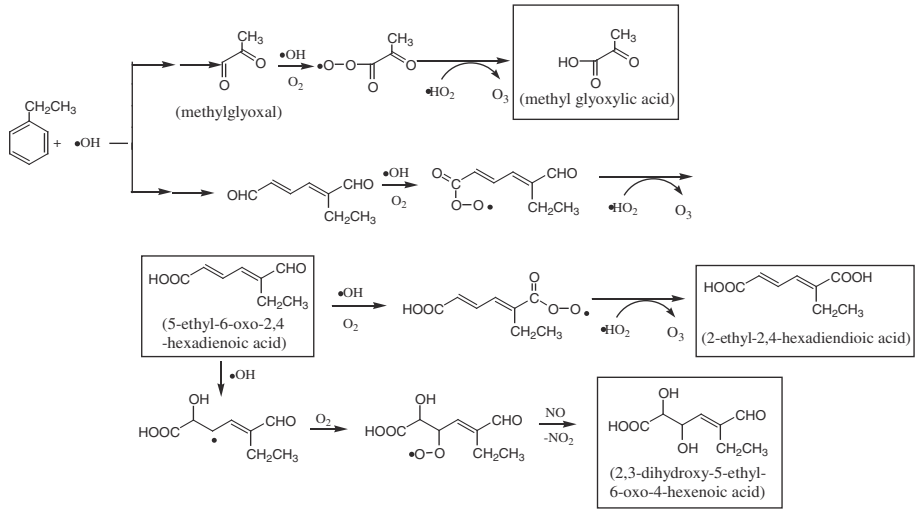

Fig. 6 – Proposed aging mechanism leading to the formation of carboxylic acid products.

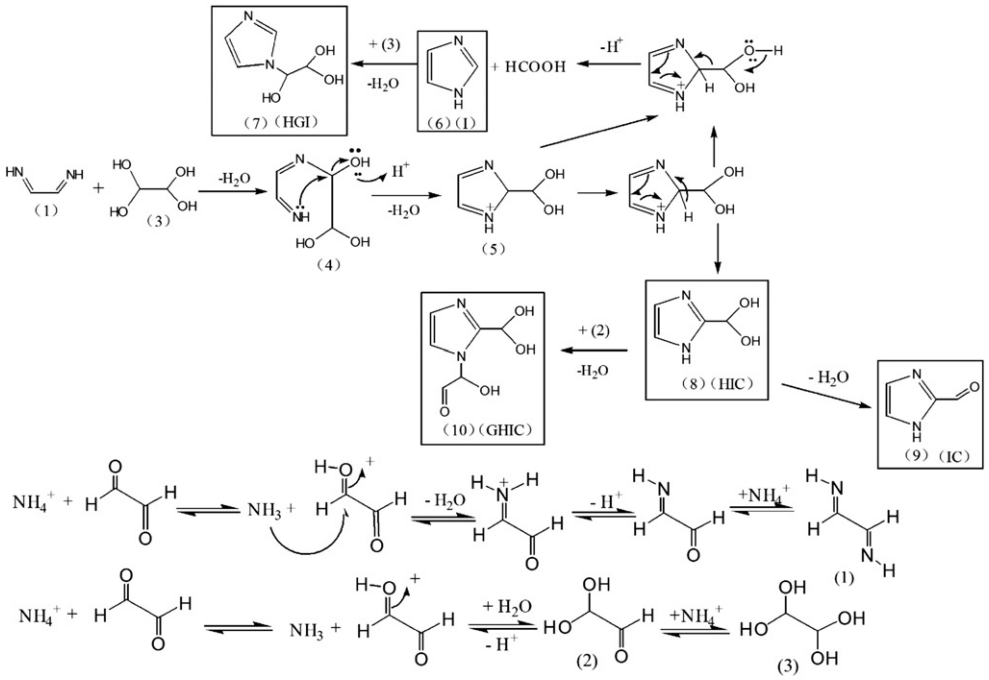

Fig. 7 – Proposed reaction mechanisms for imidazole compound formation in the aging of ethylbenzene SOA in the presence of high concentrations of $(NH_4)_2SO_4$ seed aerosol. SOA: secondary organic aerosol.

electrons of the N atom could act as a nucleophile to attack the C atom, leading to the formation of (5) after dehydration. Product (5) produces formic acid and 1H-imidazole (I) (6) through electronic rearrangement and a fracture dehydration reaction (Yu et al., 2011; Kampf et al., 2012). The formed (6) can continue to react with (3) to generate hydrated N-glyoxal-substituted 1H-imidazole (HGI) (7) after dehydration (Yu et al., 2011; Kampf et al., 2012). In addition, (5) can also undergo electron rearrangement as shown in Fig. 7 to form the hydrated 1H-imidazole-2-carbaldehyde (HIC) (8). Product (8) can be dehydrated to generate 1H-imidazole-2-carbaldehyde (IC) (9), or continue to react with (2) to form the N-glyoxal substituted hydrated 1H-imidazole-2-carbaldehyde (GHIC) (10) after dehydration (Yu et al., 2011; Kampf et al., 2012).

As displayed in Fig. 3, the mass spectra of class 14 to class 18 have many mass spectral peaks in the range of *m*/*z* 0–600, and the 18th class displays maximum *m*/*z* up to 600, indicating that high-molecular-weight (HMW) products are present in the aged ethylbenzene SOA particles in the presence of high mass concentrations of $(NH_4)_2SO_4$ seed aerosol. As mentioned before, the retention of water on the $(NH_4)_2SO_4$ particles creates ammonium ion, which can promote the formation of HMW products through heterogeneous reactions such as hydration and polymerization of aldehydes from OH-initiated oxidation of ethylbenzene (Jang et al., 2002; Gross et al., 2006). As shown in Fig. 8, the generated glyoxal could condense on existing $(NH_4)_2SO_4$ seed aerosol, and be hydrated to form a diol product (i) and tetrol product (ii). Two diol products (i) can react through nucleophilic attack of an OH group on the reactive carbonyl of the neighboring molecule to produce a five-membered 1,3-dioxalane ring product (iii), which can then react with a third diol product (i), forming the stable glyoxal trimer (which contains two dioxolane rings) (iv) (Kua et al., 2008). The formed glyoxal trimer (iv) can continue to react with diol products (i) to generate HMW products. Similarly, diol products (i) may react with tetrol product (ii) to form (v) and (vi) after dehydration and cyclization, respectively. Product (vi) can continue to react with (i) to generate HMW products. Similar to glyoxal, 2-ethyl-6-oxo-2,4-hexadienal and benzaldehyde could be hydrated to form diol products (vii) and (viii), respectively. The cross-reactions of (vii) and (viii) with (v) produce (ix) and (x), respectively (Kalberer et al., 2004). Products (ix) and (x) can continue to react with diol product (i) to generate various HMW products as outlined in Fig. 8.

To test whether and how the high concentrations of $(NH_4)_2SO_4$ seed aerosol affect the chemical composition of the aged SOA, the aging of ethylbenzene SOA in the absence and presence of 100, 200 and 300 μg/m^3 of $(NH_4)_2SO_4$ seed aerosol was performed. About 6500 pieces of single particle mass spectra of the aged ethylbenzene SOA particles for each experiment were obtained and processed with the FCM algorithm as described above. The Davies–Bouldin index and the determined spectral patterns as the cluster centers for the aged ethylbenzene SOA particles in the presence of different concentrations of $(NH_4)_2SO_4$ seed aerosol after 24 hr photooxidation are shown in Figs. S7–S10 in Appendix A. Supplementary data. The FCM clustering results show that imidazole compounds and HMW products were detected in the aged ethylbenzene SOA particles in the presence of high concentrations of $(NH_4)_2SO_4$ seed aerosol, indicating that high concentrations of dry $(NH_4)_2SO_4$ seed aerosol can promote the formation of imidazole compounds and HMW products in the aged ethylbenzene SOA. Especially for HMW products, *m*/*z* increases gradually with increasing concentrations of $(NH_4)_2SO_4$ seed aerosol. HMW products with maximum *m*/*z*

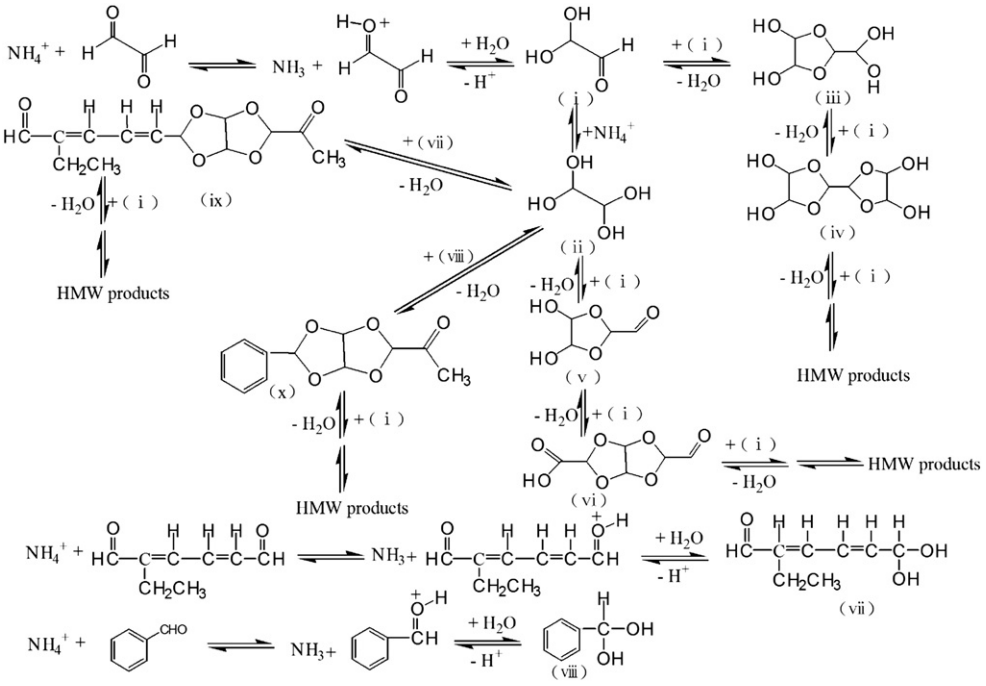

Fig. 8 – Proposed reaction mechanisms for high-molecular-weight product formation in the aging of ethylbenzene SOA in the presence of high concentrations of $(NH_4)_2SO_4$ seed aerosol. SOA: secondary organic aerosol.

up to 630 were measured in the aged ethylbenzene SOA particles in the presence of 300 μg/m^3 $(NH_4)_2SO_4$ seed aerosol.

As proposed by Lu et al. (2009), the thickness of the organic layer coating plays an important role in SOA formation. With the same amount of SOA generation, the seed surface concentration is approximately inversely proportional to the thickness of the organic layer. With the same amount of ethylbenzene SOA generation, a high concentration of $(NH_4)_2SO_4$ seed aerosol enables a thin organic layer. $(NH_4)_2SO_4$ seed aerosol may produce ammonium ion by absorbing water from its outer organic layer coating. Also, a high concentration of $(NH_4)_2SO_4$ aerosol provides more reactive sites for heterogeneous reactions. Thus, the $(NH_4)_2SO_4$ seed aerosol induces the ammonium-catalyzed heterogeneous reactions, such as hydration and polymerization of aldehydes from OH-initiated oxidation of ethylbenzene, and facilitates formation of HMW products as mentioned above, and the thinner the organic layer is, the more pronounced the HMW product formation enhancement by the $(NH_4)_2SO_4$ seed aerosol is.

2.4. Comparison with previous aromatic SOA aging studies

Sato et al. (2012) and Huang et al. (2014) have used LC–MS and ALTOFMS to measure the particulate products of aged benzene SOA in the absence of inorganic seed aerosol. Nitrogenated organic compounds and oxocarboxylic acids are observed as major aging products. Compared to the experiments of Sato et al. (2012) and Huang et al. (2014), our work characterized aged ethylbenzene SOA in the presence of high concentrations of $(NH_4)_2SO_4$ seed aerosol in real-time. The chemical composition of the aged ethylbenzene SOA obtained by ALTOFMS coupled with the FCM clustering algorithm suggested that in addition to nitrogenated organic compounds and oxocarboxylic acids, imidazole compounds and HMW products are also predominant products in the aged particles. Although the concentrations of ethylbenzene and NO_x in our smog experiments are several orders of magnitude higher than that in the ambient atmosphere, the effect of high concentrations of $(NH_4)_2SO_4$ seed aerosol is still expected to be important in the atmosphere since the atmospheric organic aerosol mass loading is low, under which condition the incidence of the $(NH_4)_2SO_4$ effect could be high. Studies (Yu et al., 2011; Kampf et al., 2012; Nakayama et al., 2013) have shown that imidazole compounds and HMW products can absorb solar radiation in the ultraviolet–visible effectively, resulting in a decrease in air visibility. These findings provide new information for discussing aromatic SOA aging mechanisms.

3. Conclusions

A laboratory study was carried out to investigate the particulate products of aged ethylbenzene SOA particles in the presence of high mass (100–300 μg/m^3) concentrations of $(NH_4)_2SO_4$ seed aerosol using the aerosol laser time-of-flight mass spectrometer detection approach coupled with the Fuzzy C-Means data processing algorithm in real-time. This on-line detection method gives rise to detailed chemical information about the detected single particles and the particle classes determined. Aromatic nitrogen-containing organic compounds, oxocarboxylic acids, imidazole compounds and high-molecular-weight compounds were measured as the major components in the aged SOA particles. The newly detected imidazole compounds can absorb solar radiation effectively. The optical properties of the aged aromatic SOA should be addressed in further experimental investigations.

Acknowledgments

This work was supported by the National Natural Science Foundation of China (Nos. 41575118, 41305109, 21502086, 41575126), the Outstanding Youth Science Foundation of Fujian Province of China (No. 2015J06009) and the Natural Science Foundation of Fujian Province of China (No. 2015J05028). Also, the authors express our gratitude to the referees for their valuable comments.

Appendix A. Supplementary data

Supplementary data to this article can be found online at http://dx.doi.org/10.1016/j.jes.2015.11.033.

REFERENCES

Alfarra, M.R., Paulsen, D., Gysel, M., Garforth, A.A., Dommen, J., Prévôt, A.S.H., et al., 2006. A mass spectrometric study of secondary organic aerosols formed from the photooxidation of anthropogenic and biogenic precursors in a reaction chamber. Atmos. Chem. Phys. 6 (12), 5279–5293.

Andreae, M.O., 2009. A new look at aging aerosols. Science 326 (5959), 1493–1494.

Atkinson, R., Carter, W.P.L., Winer, A.M., 1981. An experimental protocol for the determination of OH radical rate constants with organics using methyl nitrite photolysis as an OH radical source. J. Air Pollut. Control Assoc. 31 (10), 1090–1092.

Balkanski, Y.J., Jacob, D.J., Gardner, G.M., Graustein, W.C., Turekian, K.K., 1993. Transport and residence times of tropospheric aerosols inferred from a global three-dimensional simulation of ^{210}Pb. J. Geophys. Res. 98 (D11), 20573–20586.

Baltensperger, U., 2010. Aerosols in clearer focus. Science 329 (5998), 1474–1475.

Bezdek, J.C., 1981. Pattern Recognition With Fuzzy Objective Function Algorithms. Plenum Press, New York, pp. 43–93.

Bolden, A.L., Kwiatkowski, C.F., Colborn, T., 2015. New look at BTEX: are ambient levels a problem? Environ. Sci. Technol. 49 (9), 5261–5276.

Bowman, F.M., Odum, J.R., Seinfeld, J.H., Pandis, S.N., 1997. Mathematical model for gas–particle partitioning of secondary organic aerosols. Atmos. Environ. 31 (23), 3921–3931.

Correa, S.M., Arbilla, G., Marques, M.R.C., Oliveira, K.M.P.G., 2012. The impact of BTEX emissions from gas stations into the atmosphere. Atmos. Pollut. Res. 3 (2), 163–169.

Forstner, H.J.L., Flagan, R.C., Seinfeld, J.H., 1997. Secondary organic aerosol from the photooxidation of aromatic hydrocarbons: molecular composition. Environ. Sci. Technol. 31 (5), 1345–1358.

Garland, R.M., Wise, M.E., Beaver, M.R., DeWitt, H.L., Aiken, A.C., Jimenez, J.L., et al., 2005. Impact of palmitic acid coating on the water uptake and loss of ammonium sulfate particles. Atmos. Chem. Phys. 5 (7), 1951–1961.

Gross, D.S., Gälli, M.E., Kalberer, M., Prevot, A.S.H., Dommen, J., Alfarra, M.R., et al., 2006. Real-time measurement of oligomeric species in secondary organic aerosol with the aerosol time-of-flight mass spectrometer. Anal. Chem. 78 (7), 2130–2137.

He, K.B., Yang, F.M., Ma, Y.L., Zhang, Q., Yao, X.H., Chan, C.K., et al., 2001. The characteristics of $PM_{2.5}$ in Beijing, China. Atmos. Environ. 35 (29), 4959–4970.

Henry, K.M., Donahue, N.M., 2012. Photochemical aging of alpha-pinene secondary organic aerosol: effects of OH radical sources and photolysis. J. Phys. Chem. A 116 (24), 5932–5940.

Huang, M.Q., Zhang, W.J., Hao, L.Q., Wang, Z.Y., Zhao, W.W., Gu, X.J., et al., 2007. Laser desorption/ionization mass spectrometric study of secondary organic aerosol formed from the photooxidation of aromatics. J. Atmos. Chem. 58 (3), 237–252.

Huang, M.Q., Zhang, W.J., Hao, L.Q., Wang, Z.Y., Fang, L., Kong, R.H., et al., 2010. Experimental study of photooxidation products of ethylbenzene. J. Environ. Sci. 22 (10), 1570–1575.

Huang, M.Q., Zhang, W.J., Gu, X.J., Hu, C.J., Zhao, W.X., Wang, Z.Y., et al., 2012. Size distribution and chemical composition of secondary organic aerosol formed from Cl-initiated oxidation of toluene. J. Environ. Sci. 24 (5), 860–864.

Huang, M.Q., Hao, L.Q., Guo, X.Y., Hu, C.J., Gu, X.J., Zhao, W.X., et al., 2013. Characterization of secondary organic aerosol particles using aerosol laser time-of-flight mass spectrometer coupled with FCM clustering algorithm. Atmos. Environ. 64, 85–94.

Huang, M.Q., Lin, Y.H., Huang, X.Y., Liu, X.Q., Hu, C.J., Gu, X.J., et al., 2014. Chemical analysis of aged benzene secondary organic aerosol using aerosol laser time-of-flight mass spectrometer. J. Atmos. Chem. 71 (3), 213–224.

Huang, M.Q., Lin, Y.H., Huang, X.Y., Liu, X.Q., Guo, X.Y., Hu, C.J., et al., 2015. Experimental study of particulate products for aging of 1,3,5-trimethylbenzene secondary organic aerosol. Atmos. Pollut. Res. 6 (2), 209–219.

Jang, M., Czoschke, N.M., Lee, S., Kamens, R.M., 2002. Heterogeneous atmospheric aerosol production by acid-catalyzed particle-phase reactions. Science 298 (5594), 814–817.

Kalberer, M., Paulsen, D., Sax, M., Steinbacher, M., Dommen, J., Prevot, A.S.H., et al., 2004. Identification of polymers as major components of atmospheric organic aerosols. Science 303 (5664), 1659–1662.

Kampf, C.J., Jakob, R., Hoffmann, T., 2012. Identification and characterization of aging products in the glyoxal/ammonium sulfate system — implications for light-absorbing material in atmospheric aerosols. Atmos. Chem. Phys. 12 (14), 6323–6333.

Kane, D.B., Johnston, M.V., 2001. Enhancing the detection of sulfate particles for laser ablation aerosol mass spectrometry. Anal. Chem. 73 (22), 5365–5369.

Kua, J., Hanley, S.W., De Haan, D.O., 2008. Thermodynamics and kinetics of glyoxal dimer formation: a computational study. J. Phys. Chem. A 112 (1), 66–72.

Lan, T.T.N., Minh, P.A., 2013. BTEX pollution caused by motorcycles in the megacity of HoChiMinh. J. Environ. Sci. 25 (2), 348–356.

Lee, H.J., Aiona, P.K., Laskin, A., Laskin, J., Nizkorodov, S.A., 2014. Effect of solar radiation on the optical properties and molecular composition of laboratory proxies of atmospheric brown carbon. Environ. Sci. Technol. 48 (17), 10217–10226.

Loza, C.L., Chhabra, P.S., Yee, L.D., Craven, J.S., Flagan, R.C., Seinfeld, J.H., 2012. Chemical aging of m-xylene secondary organic aerosol: laboratory chamber study. Atmos. Chem. Phys. 12 (1), 151–167.

Lu, Z.F., Hao, J.M., Takekawa, H., Hu, L.H., Li, J.H., 2009. Effect of high concentrations of inorganic seed aerosols on secondary organic aerosol formation in the m-xylene/NO_x photooxidation system. Atmos. Environ. 43 (4), 897–904.

Meyer, N.K., Duplissy, J., Gysel, M., Metzger, A., Dommen, J., Weingartner, E., et al., 2009. Analysis of the hygroscopic and volatile properties of ammonium sulphate seeded and unseeded SOA particles. Atmos. Chem. Phys. 9 (2), 721–732.

Nakayama, T., Sato, K., Matsumi, Y., Imamura, T., Yamazaki, A., Uchiyama, A., 2013. Wavelength and NO_x dependent complex refractive index of SOAs generated from the photooxidation of toluene. Atmos. Chem. Phys. 13 (2), 531–545.

Ng, N.L., Canagaratna, M.R., Jimenez, J.L., Chhabra, P.S., Seinfeld, J.H., Worsnop, D.R., 2011. Changes in organic aerosol composition with aging inferred from aerosol mass spectra. Atmos. Chem. Phys. 11 (13), 6465–6474.

Nozière, B., Dziedzic, P., Córdova, A., 2009. Products and kinetics of the liquid-phase reaction of glyoxal catalyzed by ammonium ions (NH_4^+). J. Phys. Chem. A 113 (1), 231–237.

Rincón, A.G., Guzmán, M.I., Hoffmann, M.R., Colussi, A.J., 2009. Optical absorptivity versus molecular composition of model organic aerosol matter. J. Phys. Chem. A 113 (39), 10512–10520.

Robinson, A.L., Donahue, N.M., Shrivastava, M.K., Weitkamp, E.A., Sage, A.M., Grieshop, A.P., et al., 2007. Rethinking organic aerosols: semivolatile emissions and photochemical aging. Science 315 (5816), 1259–1262.

Robinson, C.B., Schill, G.P., Zarzana, K.J., Tolbert, M.A., 2013. Impact of organic coating on optical growth of ammonium sulfate particles. Environ. Sci. Technol. 47 (23), 13339–13346.

Rudich, Y., Donahue, N.M., Mentel, T.F., 2007. Aging of organic aerosol: bridging the gap between laboratory and field studies. Annu. Rev. Phys. Chem. 58 (1), 321–352.

Sareen, N., Moussa, S.G., McNeill, V.F., 2013. Photochemical aging of light-absorbing secondary organic aerosol material. J. Phys. Chem. A 117 (14), 2987–2996.

Sato, K., Takami, A., Isozaki, T., Hikida, T., Shimono, A., Imamura, T., 2010. Mass spectrometric study of secondary organic aerosol formed from the photo-oxidation of aromatic hydrocarbons. Atmos. Environ. 44 (8), 1080–1087.

Sato, K., Takami, A., Kato, Y., Seta, T., Fujitani, Y., Hikida, T., et al., 2012. AMS and LC/MS analyses of SOA from the photooxidation of benzene and 1,3,5-trimethyl benzene in the presence of NO_x: effects of chemical structure on SOA aging. Atmos. Chem. Phys. 12 (10), 4667–4682.

Schnitzler, E.G., Dutt, A., Charbonneau, A.M., Olfert, J.S., Jäger, W., 2014. Soot aggregate restructuring due to coatings of secondary organic aerosol derived from aromatic precursors. Environ. Sci. Technol. 48 (24), 14309–14316.

Schreier, S.F., Peters, E., Richter, A., Lampel, J., Wittrock, F., Burrows, J.P., 2015. Ship-based MAX-DOAS measurements of tropospheric NO_2 and SO_2 in the South China and Sulu Sea. Atmos. Environ. 102, 331–343.

Silva, P.J., Prather, K.A., 2002. Interpretation of mass spectra from organic compounds in aerosol time-of-flight mass spectrometry. Anal. Chem. 72 (15), 3553–3562.

Singh, A., Dey, S., 2012. Influence of aerosol composition on visibility in megacity Delhi. Atmos. Environ. 62, 367–373.

Sorooshian, A., Csavina, J., Shingler, T., Dey, S., Brechtel, F.J., Saez, A.E., et al., 2012. Hygroscopic and chemical properties of aerosols collected near a copper smelter: implications for public and environmental health. Environ. Sci. Technol. 46 (17), 9473–9480.

Tong, D.L., Xu, R.K., 2012. Effects of urea and $(NH_4)_2SO_4$ on nitrification and acidification of ultisols from southern China. J. Environ. Sci. 24 (4), 682–689.

Topinka, J., Rossner Jr., P., Milcova, A., Schmuczerova, J., Svecova, V., Sram, R.J., 2011. DNA adducts and oxidative DNA damage induced by organic extracts from PM2.5 in an acellular assay. Toxicol. Lett. 202 (3), 186–192.

Tritscher, T., Dommen, J., DeCarlo, P.F., Gysel, M., Barmet, P.B., Praplan, A.P., et al., 2011. Volatility and hygroscopicity of aging secondary organic aerosol in a smog chamber. Atmos. Chem. Phys. 11 (22), 11477–11496.

Updyke, K.M., Nguyen, T.B., Nizkorodov, S.A., 2012. Formation of brown carbon via reactions of ammonia with secondary organic aerosols from biogenic and anthropogenic precursors. Atmos. Environ. 63, 22–31.

Wang, Y., Zhuang, G.S., Sun, Y., An, Z.S., 2006. The variation of characteristics and formation mechanisms of aerosols in dust, haze, and clear days in Beijing. Atmos. Environ. 40 (34), 6579–6591.

Wang, S.X., Xing, J., Jang, C., Zhu, Y., Fu, J.S., Hao, J.M., 2011. Impact assessment of ammonia emissions on inorganic aerosols in east China using response surface modeling technique. Environ. Sci. Technol. 45 (21), 9293–9300.

Yu, J.Z., Jeffries, H.E., Sexton, K.G., 1997. Atmospheric photooxidation of alkylbenzenes-I. Carbonyl product analyses. Atmos. Environ. 31 (15), 2261–2280.

Yu, G., Bayer, A.R., Galloway, M.M., Korshavn, K.J., Fry, C.G., Keutsch, F.N., 2011. Glyoxal in aqueous ammonium sulfate solutions: products, kinetics and hydration effects. Environ. Sci. Technol. 45 (15), 6336–6342.

Ziemann, P.J., Atkinson, R., 2012. Kinetics, products, and mechanisms of secondary organic aerosol formation. Chem. Soc. Rev. 41 (19), 6582–6605.